Short-range-order types in binary alloys: a reflection of coherent phase stability

2000 J. Phys.: Condens. Matter 12 2749

(http://iopscience.iop.org/0953-8984/12/12/314)

J. Phys.: Condens. Matter **12** (2000) 2749–2768. Printed in the UK PII: S0953-8984(00)09156-6

Short-range-order types in binary alloys: a reflection of coherent phase stability

C Wolverton†, V Ozoliņš‡ and Alex Zunger§

† Ford Research Laboratory, MD3028/SRL, Dearborn, MI 48121-2053, USA
‡ Sandia National Laboratories, Livermore, CA 94551, USA
§ National Renewable Energy Laboratory, Golden, CO 80401, USA

Received 1 November 1999

Abstract. The short-range order (SRO) present in disordered solid solutions is classified according to three characteristic system-dependent energies: (1) formation enthalpies of ordered compounds, (2) enthalpies of mixing of disordered alloys, and (3) the energy of coherent phase separation (the composition-weighted energy of the constituents each constrained to maintain a common lattice constant along an A/B interface). These energies are all compared against a common reference, the energy of incoherent phase separation (the composition-weighted energy of the constituents each at their own equilibrium volumes). Unlike long-range order (LRO), short-range order is determined by energetic competition between phases *at a fixed composition*, and hence only *coherent* phase-separated states are of relevance for SRO. We find five distinct SRO types, and give examples showing each of these five types, including Cu–Au, Al–Mg, GaP–InP, Ni–Au, and Cu–Ag. The SRO is calculated from first principles using the mixed-space cluster expansion approach combined with Monte Carlo simulations. Additionally, we examine the effect of inclusion of coherency strain in the calculation of SRO, and specifically examine the appropriate functional form for accurate SRO calculations.

1. Introduction: short-range order and coherent phase stability

The equilibrium regions involved in solid-state binary alloy phase diagrams are ordered phases, two-phase regions, and disordered solid solutions. The latter form at elevated temperatures, and consist of an $A_{1-x}B_x$ phase in which the A and B atoms of the alloy are distributed in a disordered fashion on the sites of a single, underlying lattice (often a Bravais lattice, e.g., fcc). In the disordered phase, the atomic-scale occupation of sites of the lattice by A and B atoms does not occur perfectly randomly, nor does it occur with any long-range atomic ordering. Instead, local ordering or local clustering takes place in this solid solution, and is collectively referred to as short-range order (SRO). The degree and type of SRO in a solid solution can be quantified by specifying the Warren–Cowley SRO parameters, α_{lmn}, for a given composition (x) and temperature (T):

$$\alpha_{lmn}(x, T) = 1 - \frac{P_{lmn}^{\mathrm{A(B)}}(x, T)}{x}. \tag{1}$$

Here, $P_{lmn}^{\mathrm{A(B)}}(x, T)$ is the conditional probability that given an A atom at the origin, there is a B atom at shell (lmn). This probability is necessarily dependent on composition and temperature, thus giving an x- and T-dependence to α. If the lattice sites are occupied completely at random, the conditional probability $P(x, T)$ is equal to x, and thus $\alpha = 0$. Therefore, the departure of α from zero indicates the extent to which *atom–atom correlations* exist within disordered

0953-8984/00/122749+20$30.00

alloys. Ordering-type correlations (the predominance of A–B bonds) manifest themselves as $\alpha < 0$ while clustering-type correlations (the predominance of A–A and B–B bonds) manifest themselves as $\alpha > 0$.

In diffraction experiments, short-range order does not give rise to superstructure reflections (as in the case of long-range order), and hence one must look 'under' or 'between' the Bragg diffraction peaks to observe SRO. The SRO gives rise to modulations in the monotonic Laue background, and using diffuse scattering techniques (e.g., see references [1–7]) one can examine these modulations between the Bragg peaks. By analysing the diffuse scattered intensity, one can extract the portion, $I^{\mathrm{SRO}}_{\mathrm{diffuse}}$, of the diffuse scattering due to SRO, which is proportional to the lattice Fourier transform of the Warren–Cowley parameters:

$$I^{\mathrm{SRO}}_{\mathrm{diffuse}} \propto \alpha(x, \boldsymbol{k}) = \sum_{lmn}^{n_{\mathrm{R}}} \alpha_{lmn}(x) \mathrm{e}^{\mathrm{i}\boldsymbol{k}\cdot\boldsymbol{R}_{\mathrm{lmn}}}. \tag{2}$$

The connection between high-temperature SRO in the disordered phase and the low-temperature structures is fascinating [3, 8, 9]. As one cools the disordered phase, it eventually gives way to long-range order (LRO), either in the form of ordered compounds or phase separation. Are the SRO fluctuations of the high-temperature disordered phase simply 'precursors' or 'remnants' of the underlying LRO in the low-temperature phase, or can there be a competition between local ordering/clustering versus long-range ordering/clustering? This question can be phrased more quantitatively as follows. The maximum of equation (2) indicates the dominant wavevector $\boldsymbol{k}_0^{\mathrm{SRO}}$ for SRO fluctuations in the disordered phase. Long-range order at low T is often similarly characterized by an ordered structure composed of a dominant composition wave, $\boldsymbol{k}_0^{\mathrm{LRO}}$ [10, 11]. The question is then: What is the relationship between $\boldsymbol{k}_0^{\mathrm{SRO}}$ and $\boldsymbol{k}_0^{\mathrm{LRO}}$? Although in many cases $\boldsymbol{k}_0^{\mathrm{SRO}} = \boldsymbol{k}_0^{\mathrm{LRO}}$, there are many examples [3, 8, 9] where the dominant wavevectors of SRO and LRO do not coincide†. Some of these cases of distinct wavevectors can be explained [8] by noting that whereas SRO is determined by the energetic competition between all possible phases *at a fixed composition*, LRO stability is determined by the energy relative to all possible mixtures of phases, *even those at different compositions*.

2. Qualitative understanding of LRO versus SRO

To understand the distinction between fixed-composition and global stability, and the concomitant differences between SRO and LRO, we define three characteristic energies:

(*a*) *The formation enthalpy of an ordered (O) structure* is the (zero-pressure) total energy $E_{\mathrm{O}}(\sigma, a_\sigma)$ of the ordered phase σ with lattice constant a_σ, taken with respect to equivalent amounts of the A and B constituents, each at their 'natural', equilibrium lattice constants a_{A} and a_{B}, respectively:

$$\Delta H_{\mathrm{O}} = E_{\mathrm{O}}(\sigma, a_\sigma) - [(1-x)E_{\mathrm{A}}(a_{\mathrm{A}}) + xE_{\mathrm{B}}(a_{\mathrm{B}})]. \tag{3}$$

(*b*) *The mixing enthalpy of a random (R) alloy* is the analogous energy difference for the random alloy:

$$\Delta H_{\mathrm{R}} = E_{\mathrm{R}}(\mathrm{R}, a_\sigma) - [(1-x)E_{\mathrm{A}}(a_{\mathrm{A}}) + xE_{\mathrm{B}}(a_{\mathrm{B}})] \tag{4}$$

Notice that in both equations (3) and (4) the reference energies are those of A at its lattice constant a_{A} and B at a_{B}. For alloys with lattice-mismatched constituents ($a_{\mathrm{A}} \neq a_{\mathrm{B}}$),

† We note that the distinction between coherent and incoherent phase stability only accounts for *some* of the cases for which long- and short-range order do not coincide. Other cases illustrating the distinction between long-range order and short-range order have been found, where contributions to the free energy such as configurational entropy, geometric frustration or electron–hole free energy can differentiate energetics at low temperature (LRO) and at high temperature (SRO).

incoherent mixtures of phases with different volumes often contain misfit dislocations at the interfaces between the two phases to relieve strain. Thus, the reference energies of equations (3) and (4) involve a state of phase separation (A + B) which is incoherent. Thus, we define the incoherent phase-separated (IPS) state as

$$E_{\mathrm{IPS}} = [(1-x)E_{\mathrm{A}}(a_{\mathrm{A}}) + xE_{\mathrm{B}}(a_{\mathrm{B}})] \tag{5}$$

and this is simply chosen as the zero reference energy for our comparisons. In contrast, *coherent* two-phase mixtures contain no such misfit dislocations, and thus both phases are somewhat strained due to this constraint of coherency. This leads to:

(*c*) *The coherent phase-separated state* or coherency strain (CS), which involves strain in the plane of the interface and relaxation of the atoms perpendicular to the interface. Thus, the strain energy necessary to maintain coherency at an interface between A and B (called the 'coherency strain') is necessarily dependent on the orientation of the interface $\hat{k}$. $\Delta E_{\mathrm{CS}}(\hat{k}, x)$, the coherency strain energy, is defined as the energy change when the bulk solids A and B are deformed from their equilibrium cubic lattice constants a_{A} and a_{B} to a common lattice constant $a_{\perp}$ in the direction perpendicular to $\hat{k}$, while they are relaxed in the direction parallel to $\hat{k}$†:

$$\Delta E_{\mathrm{CS}}(\hat{k}, x) = \min_{a_{\perp}} \left[(1-x)\,\Delta E_{\mathrm{A}}^{\mathrm{epi}}(\hat{k}, a_{\perp}) + x\,\Delta E_{\mathrm{B}}^{\mathrm{epi}}(\hat{k}, a_{\perp}) \right] \tag{6}$$

where $\Delta E_{\mathrm{A}}^{\mathrm{epi}}(\hat{k}, a_{\perp})$ is the energy required to deform A biaxially to $a_{\perp}$. Each of the energies $\Delta E_{\mathrm{A}}^{\mathrm{epi}}$ and $\Delta E_{\mathrm{B}}^{\mathrm{epi}}$ is positive definite and, hence, the coherency strain of equation (6) is positive definite. Of particular importance is the lowest attainable coherency strain

$$\Delta E_{\mathrm{CS}}^{\mathrm{min}}(x) = \min_{\hat{k}} \Delta E_{\mathrm{CS}}(\hat{k}, x) \tag{7}$$

where the minimization is performed over all directions $\hat{k}$. $\Delta E_{\mathrm{CS}}^{\mathrm{min}}(x)$ then gives the formation enthalpy of the energetically most favourable coherently phase-separated state.

Using the definitions of equations (3)–(6), we can now note that:

(1) *Long-range order is determined by incoherent phase stability*: for a *long-range-ordered* compound to be a ground state (a zero-temperature stable phase), it must be lower in energy than any other compound at that composition, as well as lower in energy than any *incoherent* two-phase mixture of phases at other compositions, including a mixture of the constituent elements. Thus, a necessary condition for a ground-state structure is that $\Delta H_{\mathrm{O}} < 0$. The formation energy ΔH_{O} of equation (3) demonstrates clearly that the long-range order, and hence the equilibrium phase diagram behaviour, is determined by incoherent phase stability.

(2) *Short-range order is determined by coherent phase stability*: the short-range order involves a single-phase field (disordered solid solution) of the phase diagram, and thus does not pertain to incoherent two-phase mixtures. Some of these cases of distinct wavevectors can be explained [8] by noting that whereas SRO is determined by the energetic competition between all possible phases *at a fixed composition*, LRO stability is determined by the energy relative to all possible mixtures of phases, *even those at different compositions*. In fact, two crucial quantities for determining the types of fluctuation which develop in disordered alloys are the 'ordering energy'

$$\delta E_{\mathrm{ord}} = \Delta H_{\mathrm{O}} - \Delta H_{\mathrm{R}} \tag{8}$$

† In the general case of a low-symmetry (e.g., high-Miller-index) interface, there are three independent plane strain components instead of just the uniform plane strain described by $a_{\perp}$ (see reference [22]). Equation (6) is exact for interfaces possessing high-symmetry axes, such as (100) and (111) in fcc-based systems.

and the 'coherent phase-separation energy'

$$\delta E_{\mathrm{CPS}} = \Delta E_{\mathrm{CS}}^{\mathrm{min}} - \Delta H_{\mathrm{R}}. \tag{9}$$

δE_{ord} (δE_{CPS}) represents the energy required to form the ordered (coherent phase-separated) state, starting from the random alloy of the same composition. Both δE_{ord} and δE_{CPS} are fixed-composition energy differences and are independent of the energy of incoherent phase separation.

Figure 1 illustrates five possible relative orders of the energies ΔH_{O}, ΔH_{R}, and ΔE_{CS} of equations (3)–(6). The ordered structures 'O' in figure 1 are representative of the lowest-energy coherent configurations, i.e., structures with dominant composition waves at the Brillouin zone boundary (e.g., the $L1_0$, $L1_1$, or $L1_2$ structures). It should be noted that in cases (e.g., Al–Cu) where the lowest-energy coherent configurations correspond to ordered compounds which have a large degree of 'clustering', one can obtain clustering-type SRO even in a 'type I' alloy (see reference [12]). In this paper, we study these types I–V of LRO/SRO behaviour in real alloy systems using a first-principles total-energy technique for calculating ΔH_{O} and ΔE_{CS}, and a cluster expansion method for calculating ΔH_{R} and SRO.

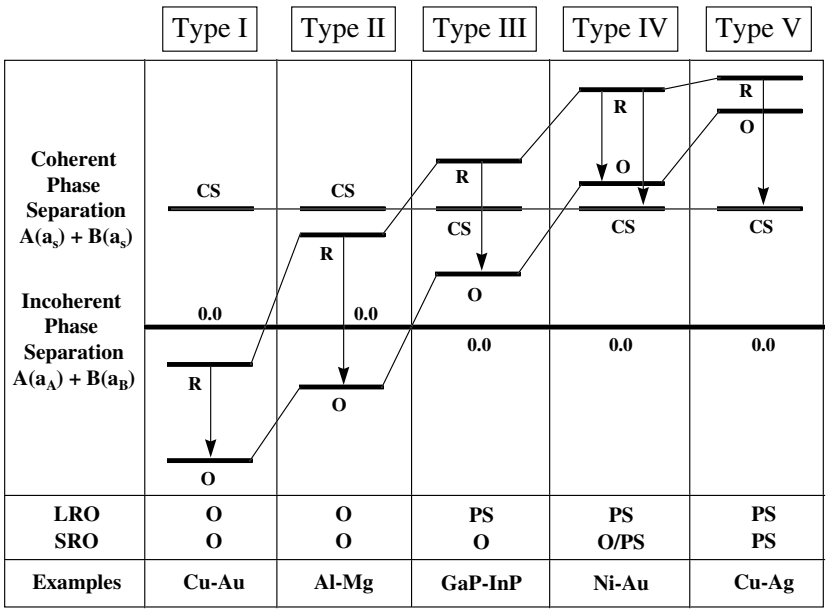

Figure 1. A schematic illustration of the classification of alloy types in terms of energies of ordered (O) compounds, random (R) alloys, and coherent phase separation, or coherency strain (CS) minimized with respect to orientation. Note that the O → R and CS → R energy differences give the ordering energy and the coherent phase-separation energy, δE_{ord} and δE_{CPS}, respectively. Energies are shown relative to the reference state of incoherent phase separation (IPS) A + B, labelled as '0.0' to indicate the zero of energy. The ordered structures 'O' are meant to be representative of the lowest-energy structures with dominant composition waves at the Brillouin zone boundary (e.g., the $L1_0$, $L1_1$, or $L1_2$ structures). It should be noted that in cases (e.g., Al–Cu) where the lowest-energy coherent configurations correspond to ordered compounds which have a large degree of 'clustering', one can obtain clustering-type SRO even in a 'type I' alloy (see reference [12]).

The salient features of the SRO are decided by the quantities δE_{ord} and δE_{CPS}, so we examine the qualitative possibilities for these two quantities, defining the five alloy types of figure 1:

type I: $\delta E_{\mathrm{ord}} < 0 < \delta E_{\mathrm{CPS}}$ (e.g., Cu–Au)
type II: $\delta E_{\mathrm{ord}} < 0 \sim \delta E_{\mathrm{CPS}}$ (e.g., Al–Mg)
type III: $\delta E_{\mathrm{ord}} < \delta E_{\mathrm{CPS}} < 0$ (e.g., GaP–InP)
type IV: $\delta E_{\mathrm{ord}} \sim \delta E_{\mathrm{CPS}} < 0$ (e.g., Ni–Au)
type V: $\delta E_{\mathrm{CPS}} < \delta E_{\mathrm{ord}} < 0$ (e.g., Cu–Ag).

The arrows in figure 1 show schematically the fluctuations in the random alloy which are energetically most favourable. In 'type I', 'type II', and 'type III' alloys, the ordered alloy is lower in energy than both the random alloy ($\delta E_{\mathrm{ord}} < 0$) and the coherent phase-separated state ($\delta E_{\mathrm{ord}} < \delta E_{\mathrm{CPS}}$). Therefore, energetic fluctuations of the random alloy are expected to be of ordering type, depicted as R $\rightarrow$ O in figure 1. Thus, the SRO of solid solutions of types I, II, and III alloys are all ordering type ($\boldsymbol{k}_{\mathrm{SRO}} \neq 0$), even though the LRO is ordering only in types I and II, but phase separating (incoherently) in type III. On the other hand, a 'type V' alloy is a prototypical 'clustering' alloy, where the coherent phase-separated state is lower in energy than both the random alloy ($\delta E_{\mathrm{CPS}} < 0$) and the ordered alloy ($\delta E_{\mathrm{CPS}} < \delta E_{\mathrm{ord}}$). Hence, the SRO is expected to be of clustering type ($\boldsymbol{k}_{\mathrm{SRO}} = 0$), represented by R $\rightarrow$ CS in figure 1. Since phase separation is the lowest-energy incoherent state in a 'type V' alloy, the LRO of this alloy is also phase separation. 'Type IV' alloys are intermediate between 'type III' and 'type V'. In type IV, there is strong competition between ordering and coherent phase separation ($\delta E_{\mathrm{ord}} \sim \delta E_{\mathrm{CPS}}$), and, thus, it is difficult to predict even the qualitative behaviour of the SRO for this case, since there are expected to be competitive energetic fluctuations simultaneously towards ordering and phase separation in these alloys (illustrated by both R $\rightarrow$ O and R $\rightarrow$ CS arrows in figure 1). As shown below, the SRO of the 'type IV' alloy, Ni–Au, is intermediate between that of a strongly ordering alloy (types I, II, and III) and that of a strongly clustering alloy (type V).

3. The mixed-space cluster expansion—a description of atomically relaxed, coherent alloy energetics

3.1. General formalism

Calculating the equilibrium SRO in solid solutions from an energetic approach requires, in principle, a statistical sampling of all configurations σ. Even a binary alloy system with a modest number of sites N possesses 2^N possible configurations, and hence the number of configurations for which we need to know the energy quickly becomes impractically large. Hence, one method used to obtain finite-T thermodynamics is to perform statistical calculations by means of a Monte Carlo algorithm using an energy functional which describes the alloy in question. The Monte Carlo calculations efficiently sample the energy in regions of configuration space where the energy is close to its thermal average. Still, Monte Carlo calculations require the alloy energy functional to be sufficiently computationally inexpensive that it is easily evaluated for very large unit cells and for many different configurations. Hence, we wish to use a method whereby one maps first-principles alloy energetics onto an energy functional which is sufficiently simple that Monte Carlo simulations become possible, but also sufficiently accurate as to reflect the atomically relaxed energetics of a wide variety of alloy configurations. Such a method, the mixed-space cluster expansion (CE), has been developed [13, 14] and applied to several alloy systems [15–19]. The CE method relies on (i) a separation of formation enthalpy into strain and chemical contributions, and (ii) a mapping of the chemical term onto a generalized Ising-like model: one selects a single, underlying parent lattice (in the case of this paper, fcc) and defines a configuration, σ, by specifying the occupations of each of the N lattice sites by an A atom or a B atom. For each configuration,

one assigns the spin-occupation variables, $\hat{S}_i = \pm 1$, to each of the N sites. Within the Ising-like description of the mixed-space CE, the positional degrees of freedom are integrated out, leaving an energy functional of spin variables only, $\hat{S}_i$, which reproduces for each configuration σ the energy of the *atomically relaxed structure*, with atomic positions at their equilibrium (zero-force, zero-stress) values.

The details of construction of this energy functional within the LDA are discussed elsewhere [13, 18], and thus we give here only the salient points. We have used full-potential, fully relaxed, linearized augmented plane-wave method [20] (LAPW) total energies in the construction of the mixed-space cluster expansions. (In the case of GaP–InP, LAPW energies were used to fit a ternary valence-force-field functional, which was in turn used to construct the mixed-space cluster expansion [21].) Details of the LAPW method typically used in these calculations, as well as the number and types of alloy structures used in the CE fit are described in reference [18].

The expression used for the formation enthalpy of any configuration σ in the mixed-space CE is

$$\Delta H(\sigma) = \sum_{\boldsymbol{k}} J(\boldsymbol{k})|S(\boldsymbol{k},\sigma)|^2 + \sum_f D_f J_f \overline{\Pi}_f(\sigma) + \frac{1}{4x(1-x)} \sum_{\boldsymbol{k}} \Delta E_{\mathrm{CS}}(\hat{k}, x)|S(\boldsymbol{k},\sigma)|^2. \tag{10}$$

$J(\boldsymbol{k})$ is the Fourier transform of the pair interaction energies, $S(\boldsymbol{k},\sigma)$ is the structure factor for σ, f is a symmetry-distinct figure comprised of several lattice sites (pairs, triplets, etc), D_f is the number of figures per lattice site, J_f is the Ising-like interaction for the figure f, and the 'lattice-averaged product' $\overline{\Pi}_f$ is defined as a product of the variables $\hat{S}_i$ over all sites of the figure f with the overbar denoting an average over all symmetry-equivalent figures of lattice sites. Our approach is based on the fact that for simple configurations σ we know the left-hand side of equation (10) quite accurately from first-principles LDA total energies, so we can solve for the interaction energies $\{J_f\}$ and $J(\boldsymbol{k})$. Thus, we incorporate, at the outset, a detailed quantum mechanical picture (LDA) for interactions, and hence for SRO. Also, we note that the total energy includes eigenvalue (or one-electron), electrostatic, and exchange–correlation terms.

The mixed-space CE of equation (10) is separated into three parts:

(i) The first summation includes *all pair figures* corresponding to pair interactions with arbitrary separation. These pair interactions are conveniently summed using the reciprocal-space concentration-wave formalism [10, 11]. $J(\boldsymbol{k})$ and $S(\boldsymbol{k},\sigma)$ are the lattice Fourier transforms of the real-space pair interactions and spin-occupation variables, J_{ij} and $\hat{S}_i$, respectively.

(ii) The second summation includes only *non-pair figures*. The real-space summation of equation (10) is over f, the symmetry-distinct non-pair figures (points, triplets, etc).

(iii) The third summation involves $\Delta E_{\mathrm{CS}}(\hat{k}, x)$, the *coherency strain energy*, defined above.

3.2. The attenuated coherency strain term

A ΔE_{CS} term is included in equation (10) to describe the elastic strain effects between lattice-mismatched phases brought into contact and strained as a result of coherency. To understand the need for this term in the cluster expansion, consider a subset of coherent two-phase configurations: long-period $n \to \infty$ superlattices $\mathrm{A}_n/\mathrm{B}_n$ with layer orientation along $\hat{k}$. These long-period structures possess small ($\boldsymbol{k} \to 0$) dominant wavevectors, but their strain energy depends on the layer orientation, and thus the *direction* of $\boldsymbol{k}$, as seen in equation (6). However,

the cluster expansion of equation (10) *without* ΔE_{CS} and with finite-ranged interactions will give [22] $\Delta H(n) \sim 1/n$ as $n \to \infty$, independent of $\hat{k}$. Thus, one must include a ΔE_{CS} term in equation (10) since this introduces the orientation dependence in coherently strained two-phase configurations, which cannot be described by short-ranged real-space interactions $J(R)$. Further, because long-period superlattices possess $\boldsymbol{k} \to 0$ dominant wavevectors, but the strain energy is dependent on the direction of $\hat{k}$, there is a $\boldsymbol{k} \to 0$ non-analyticity in the reciprocal-space description of the coherency strain. Thus, the coherency strain cannot be described everywhere by reciprocal-space interactions $J(\boldsymbol{k})$ which are analytic.

Laks *et al* [13] formulated ΔE_{CS} by ensuring that it retained the correct $n \to \infty$ superlattice limit:

$$\Delta E_{CS}(\sigma) = \frac{1}{4x(1-x)} \sum_{\boldsymbol{k}} \Delta E_{CS}(\hat{k}, x)|S(\boldsymbol{k}, \sigma)|^2. \tag{11}$$

Laks *et al* demonstrated that this form gives the correct orientation and composition dependence in the long-period limit of the coherency strain [13]. Furthermore, it was shown that this form is uniquely defined for short-period superlattices and non-superlattices. However, this form treats short-period superlattices ($\boldsymbol{k} \to 2\pi/n$) the same way that long-period superlattices ($\boldsymbol{k} \to \infty$) are treated. To generalize equation (11), we note that the $\boldsymbol{k} \to 0$ non-analyticity could still be satisfied if we were to multiply E_{CS} by a function $F(\boldsymbol{k})$:

$$\Delta E_{CS}(\sigma) = \frac{1}{4x(1-x)} \sum_{\boldsymbol{k}} \Delta E_{CS}(\hat{k}, x)|S(\boldsymbol{k}, \sigma)|^2 F(\boldsymbol{k}) \tag{12}$$

so long as $F(\boldsymbol{k}) \to 1$ as $\boldsymbol{k} \to 0$ for all directions. However, the introduction of $F(\boldsymbol{k})$ enables different treatments of short- versus long-period systems. So, the question is: Which $F(\boldsymbol{k})$ is best?

We exploit the inherent flexibility in the choice of the form of $F(\boldsymbol{k})$ to improve the convergence of the cluster expansion. Intuitively, one might expect that ΔE_{CS} of equation (12) should be related to the strain energy inherent in the structure, and thus related to the relaxation energy

$$\delta E_{rel} = E_{LDA}^{relaxed} - E_{LDA}^{unrelaxed}. \tag{13}$$

Indeed, consider the following decomposition of the formation enthalpy of any configuration σ (either ordered or random):

$$\Delta H(\sigma) = \Delta E_{VD}(\sigma) + \delta E_{chem}^{UR}(\sigma) + \delta E_{rel}(\sigma). \tag{14}$$

The first term on the right-hand side is the 'volume deformation energy', i.e., the energy required to deform the alloy constituents hydrostatically from their equilibrium lattice constants to that of the alloy structure σ. The second term is the 'chemical energy', i.e., the energy difference between the unrelaxed (UR) structure (with all atoms at ideal lattice sites) and ΔE_{VD}, so $\Delta E_{VD} + \delta E_{chem}^{UR} = \delta E_{LDA}^{UR}$. The third term, the 'relaxation energy', is the energy gained upon atomic and cell-shape distortions.

In systems where δE_{rel} is small, the CE is rapidly convergent [18]. However, large relaxations lead to long-ranged pair and multibody interactions. For an A_mB_n long-period superlattice,

$$\delta E_{rel}(A_mB_n, \hat{k}) = \Delta E_{CS}(\hat{k}, x) - \Delta E_{VD}(x). \tag{15}$$

Substituting equation (15) into equation (14), we find that

$$\Delta H(A_mB_n, \hat{k}) = \Delta E_{CS}(\hat{k}, x) + \Delta E_{chem}^{UR} \tag{16}$$

in accordance with equation (10). Equation (15) holds for infinite superlattices only, but we want a form which gives a reasonable relaxation energy for short-period ordered structures and

disordered alloys as well, i.e., we want to introduce a wavevector dependence into equation (15). Within a second-order expansion of the elastic energy, $\delta E_{\rm rel}$ can be written as [10, 11]

$$\delta E_{\rm rel}(\sigma) = -\sum_{\boldsymbol{k}} V_{\rm rel}(\boldsymbol{k})|S(\boldsymbol{k},\sigma)|^2 \tag{17}$$

where $V_{\rm rel}(\boldsymbol{k})$ can be related to the lattice Fourier transforms of the Kanzaki forces and dynamical matrix [10, 11]. We will retain the form of equation (17), but we will generalize $V_{\rm rel}(\boldsymbol{k})$ to accommodate some of the shortcomings of the second-order expansion derivation.

To gain insight into the wavevector dependence of the relaxation energy, consider the following breakdown of the relaxation energy:

$$\delta E_{\rm rel}(\sigma) = \delta E^{\rm int}_{\rm rel}(\sigma) + \delta E^{\rm ext}_{\rm rel}(\sigma). \tag{18}$$

The cell-internal relaxation $\delta E^{\rm int}_{\rm rel}$ is the energy gained when atomic positions within the unit cell are relaxed, but the unit-cell vectors maintain their ideal angles and lengths, whereas the cell-external relaxation $\delta E^{\rm ext}_{\rm rel}$ is the energy gained when the unit-cell vectors are allowed to relax. For some high-symmetry structures, $\delta E^{\rm int}_{\rm rel} = 0$ by symmetry: structures with dominant composition wavevectors at the Brillouin zone boundary often possess only cell-external degrees of freedom. For example, the A_1B_1 superlattice along (001) is tetragonal, composed of $\boldsymbol{k} = (001)$ waves, and possesses only the tetragonality ratio c/a as a symmetry-allowed degree of freedom. However, the A_2B_2 (001) superlattice is composed of $\boldsymbol{k} = \frac{1}{2}(001)$ waves, and, in addition to the c/a ratio, also possess a cell-internal degree of freedom.

It is interesting to know the extent to which cell-internal and cell-external relaxations are energetically important in various alloy systems. Table 1 shows the LAPW calculated relaxation energy for A_2B_2 and A_1B_1 (001) superlattice structures for a variety of size-mismatched noble-metal and aluminium alloy systems: Ni–Au, Cu–Au, Cu–Ag, Ni–Al, Cu–Al, and Al–Mg. The relaxation energy is decomposed into cell-internal and cell-external pieces. Table 1 demonstrates that (i) when symmetry does not prohibit cell-*internal* relaxation,

Table 1. LAPW calculated relaxation energies (equation (13)) in a variety of noble-metal and aluminium alloys. Shown are the relaxation energies for A_2B_2 (001) and A_1B_1 (001) superlattices. The former possesses both cell-internal and cell-external degrees of freedom, and the latter possesses only a cell-external degree of freedom. The fraction of the relaxation energy which comes from the cell-internal relaxation is shown, and to give some idea of the scale of the relaxation energy, the ratio between the relaxation energy and the formation enthalpy of the structure is also given.

A_2B_2 (001) superlattice			
Superlattice	$\delta E_{\rm rel}$	$\delta E^{\rm int}_{\rm rel}/\delta E_{\rm rel}$	$\lvert\delta E_{\rm rel}/\Delta H(A_2B_2)\rvert$
Ni_2Au_2	−216.5	0.88	3.08
Cu_2Au_2	−143.1	0.84	21.36
Cu_2Ag_2	−96.7	0.90	1.24
Ni_2Al_2	−303.9	0.50	0.69
Cu_2Al_2	−88.2	0.80	1.19
Al_2Mg_2	−34.6	1.00	2.52
A_1B_1 (001) superlattice			
Superlattice	$\delta E_{\rm rel}$	$\delta E^{\rm int}_{\rm rel}/\delta E_{\rm rel}$	$\lvert\delta E_{\rm rel}/\Delta H(A_1B_1)\rvert$
Ni_1Au_1	−22.0	0.0	0.29
Cu_1Au_1	−12.1	0.0	0.25
Cu_1Ag_1	−7.1	0.0	0.07
Ni_1Al_1	−141.7	0.0	0.21
Cu_1Al_1	−115.9	0.0	0.71
Al_1Mg_1	~ 0	—	~ 0

this mode of relaxation is dominant (e.g., 100% in Al_2Mg_2). Yet, (ii) cell-*external* relaxation is not negligible: it is 100% (by symmetry) for A_1B_1 along (001) or (111); it is ∼50% for (001) Cu_2Al_2, and ∼10–15% for Ni_2Au_2 and Cu_2Au_2. (iii) The A_2B_2 structure has much larger (mostly cell-internal) relaxation than the A_1B_1 structure. Similar studies [13] on longer-period A_nB_n superlattices confirm that $\delta E_{\rm rel}$ increases with n. *Thus, the cell-internal relaxation decays as the dominant wavevector* $\boldsymbol{k} \sim 1/n$ *increases towards the Brillouin zone boundary* (small-period superlattices). However, cell-external relaxation does not. In the second-order expansion approaches, it can be shown [10] that the relaxation energy decays precisely to zero at the Brillouin zone boundary. Thus, these types of approach do not account for energy lowering due to cell-*external* relaxations. For some systems (Al–Mg), this is probably an adequate assumption, while for others (Ni–Al, Cu–Al) it is not. It is possible to introduce macroscopic elastic strain into the first-principles linear response approaches [23]; however, to our knowledge this approach has not been applied to studies of bulk alloy systems. In this vein, we also note that linear response and alchemical calculations have been extended to third order [24, 25]. However, to our knowledge, none of these third-order approaches treats the effects of macroscopic elastic strain, required to describe cell-external relaxations. To obtain a non-zero relaxation energy at the Brillouin zone boundary, $V_{\rm rel}(\boldsymbol{k})$ will be given by

$$\tilde{V}_{\rm rel}(k) = \frac{\Delta E_{\rm VD}(x) - \Delta E_{\rm CS}(x, \hat{\boldsymbol{k}})}{4x(1-x)} F(\boldsymbol{k}) \tag{19}$$

where $F(\boldsymbol{k})$ is chosen such that the relaxation energy from equation (19) matches the first-principles values obtained from equation (13). We have selected [26]

$$F(\boldsymbol{k}) = \mathrm{e}^{-(|\boldsymbol{k}|/k_c)^2} \tag{20}$$

with k_c being an adjustable parameter. We find that

$$\delta E_{\rm rel}(\sigma) = -\frac{1}{2} \sum_{\boldsymbol{k}} \frac{\Delta E_{\rm VD}(x) - \Delta E_{\rm CS}(x, \hat{\boldsymbol{k}})}{4x(1-x)} |S(\sigma, \boldsymbol{k})|^2 \mathrm{e}^{-(|\boldsymbol{k}|/k_c)^2} \tag{21}$$

with $k_c \sim 0.6(2\pi/a_0)$ matches the LDA relaxation energies (e.g., table 1) of many compounds very well; hence we will use

$$\Delta E_{\rm CS}(\sigma) = \frac{1}{4x(1-x)} \sum_{\boldsymbol{k}} \Delta E_{\rm CS}(\hat{k}, x) |S(\boldsymbol{k}, \sigma)|^2 \mathrm{e}^{-(|\boldsymbol{k}|/k_c)^2} \tag{22}$$

in our cluster expansion instead of equation (11) for $E_{\rm CS}(\sigma)$. The resulting mixed-space cluster expansion then is

$$\Delta H(\sigma) = \sum_{\boldsymbol{k}} J(\boldsymbol{k}) |S(\boldsymbol{k}, \sigma)|^2 + \sum_f D_f J_f \overline{\Pi}_f(\sigma) + \frac{1}{4x(1-x)} \sum_{\boldsymbol{k}} \Delta E_{\rm CS}(\hat{k}, x) |S(\boldsymbol{k}, \sigma)|^2 \mathrm{e}^{-(|\boldsymbol{k}|/k_c)^2}. \tag{23}$$

We refer to equation (22) as the 'attenuated coherency strain'. It differs from previous calculations in the choice of $F(\boldsymbol{k})$ of equation (20) rather than $F(\boldsymbol{k}) = 1$.

To summarize this section, we find that equation (23) improves the conventional cluster expansion since the effect of strain for large-$\boldsymbol{k}$ (small-period) structures is attenuated. This will turn out to be important when *anharmonic strain is large* and when the relaxation energy of short-period $\boldsymbol{k} \to \pi/n$ structures is particularly small relative to that of long-period $\boldsymbol{k} \to 0$ structures, so treating them equally (as is the case if $F(\boldsymbol{k}) = 1$) is unbalanced. Since attenuation does not affect $\boldsymbol{k} \to 0$ energetics, it is unimportant for phase-separating systems where the SRO peaks near $\boldsymbol{k} = 0$.

We next discuss the $F(\boldsymbol{k}) = 1$ form of the coherency strain energy (equation (11)) used in the mixed-space CE of equation (23) and show how it can fail for some short-period superlattices in systems which possess strongly anharmonic strain. The failures include prediction of spurious ground-state structures, and incorrect short-range-order patterns (when compared with measured patterns). Attenuating the form of the coherency strain energy via equation (20) is shown to rectify these problems.

3.3. Attenuating the coherency strain for short-period superlattices

The problems which can arise with the unattenuated form of the CS are most easily explained with an example: Cu-rich Cu–Au alloys. This system has a very large lattice constant mismatch (12%), and thus anharmonic strain effects are significant. First-principles calculations of the coherency strain in Cu–Au alloys [18] have shown that the strong anharmonic strain of Au results in a low CS for the (201) direction in Cu-rich alloys. This simply means that (201) long-period superlattices (small $\boldsymbol{k}$) will be lower in energy than differently oriented long-period superlattices. However, this energetic preference for (201) structures does not necessarily hold for short-period superlattices (large $\boldsymbol{k}$), due to the first two terms of equation (10) which describe interfacial energies of atoms near the Cu/Au interfaces. But the unattenuated form of the coherency strain energy given in equation (11) will give a large energy lowering to *any* Cu-rich structure which possesses composition waves lying along the (210) direction, regardless of the *magnitude* of the wave (the superlattice period). Thus, the short-period Cu_4Au_1 superlattice along (210), which is a structure composed of composition waves at the origin and $\boldsymbol{k} = \frac{2}{5}(210)$ (a rather large $\boldsymbol{k}$, 80% of the way to the Brillouin zone boundary) will be given a low energy by equation (11) due to the low energy of the small-$\boldsymbol{k}$ long-period (210) superlattices†. This is illustrated in figure 2 which shows the unattenuated ($F = 1$) and attenuated cluster expansion predictions for the formation enthalpy of this Cu_4Au_1 structure as well as the directly calculated LAPW formation enthalpy. The SRO of $Cu_{0.9}Au_{0.1}$ is shown in figure 3 as calculated from the unattenuated and attenuated CE, as well as as obtained from diffuse scattering measurements [27]. The $F = 1$ unattenuated CE has the following features:

(1) The Cu_4Au_1 (210) superlattice is artificially low in energy due to the low (210) CS energy (figure 2).
(2) The $F = 1$ cluster expansion incorrectly predicts this structure's energy to lie below the tie line connecting Cu_3Au ($L1_2$) and Cu, in disagreement with both experiment and direct LAPW calculations.
(3) As we see from figure 3, the unattenuated $F = 1$ cluster expansion predicts (210)-type SRO in the solid solution for Cu-rich alloys. The predicted SRO along the (210) direction is due to the low (210) long-period superlattice energy for Cu-rich alloys. However, the measured SRO pattern [27] shows peaks at the (100) points.

The effects of attenuating the CS are significant:

(1) The form of $F(\boldsymbol{k})$ of equation (20) progressively attenuates the CS for structures with larger wavevectors. Thus, in our example, the energy of the *short*-period Cu_4Au_1 superlattice is not given an artificially large relaxation energy due to the large relaxation energy of the *long*-period (210) superlattices. Consequently, its energy is raised significantly, in excellent agreement with direct LAPW calculations (figure 2), despite the fact that this energy was not used in fitting either the attenuated or unattenuated CE.

† It is important to note that the anharmonic CS is *correct* near the origin of reciprocal space, or for long-period Cu/Au superlattices (i.e., within LDA, 201 is really the softest elastic direction for highly distorted Au); the use of the soft 201 direction for wavevectors away from the origin is where the problems of the unattenuated CE arise.

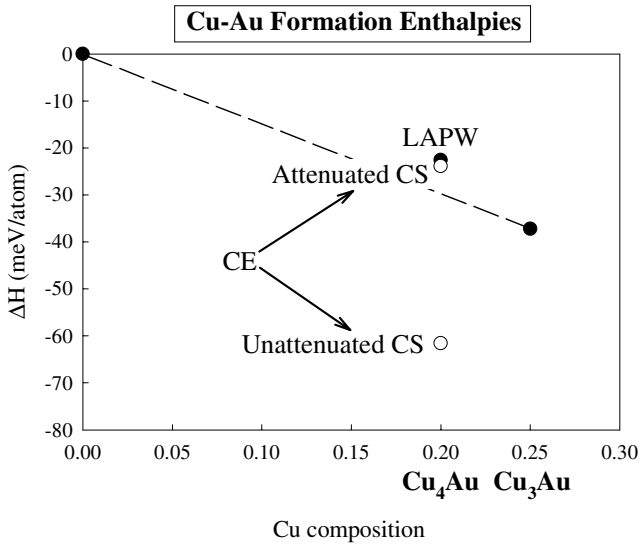

Figure 2. Energetics of the Cu_4Au_1 (210) superlattice relative to Cu_3Au ($L1_2$) and Cu.

(2) The energy of Cu_4Au_1 is brought above the tie line connecting Cu_3Au + Cu; thus, attenuating the CS solves the problem of false ground states due to low-energy long-period strain energies.

(3) Figure 3 shows that the SRO pattern is brought into quantitative agreement with experiment by the attenuation. Calculated peaks in the SRO move from the (210) direction to the (100) direction upon attenuation of the CS.

Thus, we see that the form of the attenuated coherency strain is most likely to be crucial in ordering systems (where wavevectors away from the origin are important) which possess highly anharmonic strain energies (where the soft elastic direction can shift as a function of composition).

Next, we discuss the short-range-order behaviour for a series of alloys classified according to their energetics as in figure 1. We show that the Al–Mg system represents a type II alloy, which has not previously been discussed. We specifically point out the strong effect of attenuating the CS for the Cu–Au and Ni–Au systems, and show that the attenuated strain leads to SRO in Cu-rich Cu–Au alloys in agreement with experiment and significantly changes the predicted SRO in Ni-rich Ni–Au, for which there are currently no measurements.

4. Short-range-order types

We now investigate the SRO/LRO types of figure 1. The calculations for some of these alloy systems (Cu–Au, Ni–Au, and Cu–Ag) have been discussed previously [15] using the unattenuated $F = 1$ form of the coherency strain. Thus, for these alloys, we do not provide a detailed account of the experimental and theoretical literature on the SRO of these solid solutions. Rather, we discuss the effects of attenuating the coherency strain on the SRO, and compare with experimental diffuse scattering measurements where appropriate.

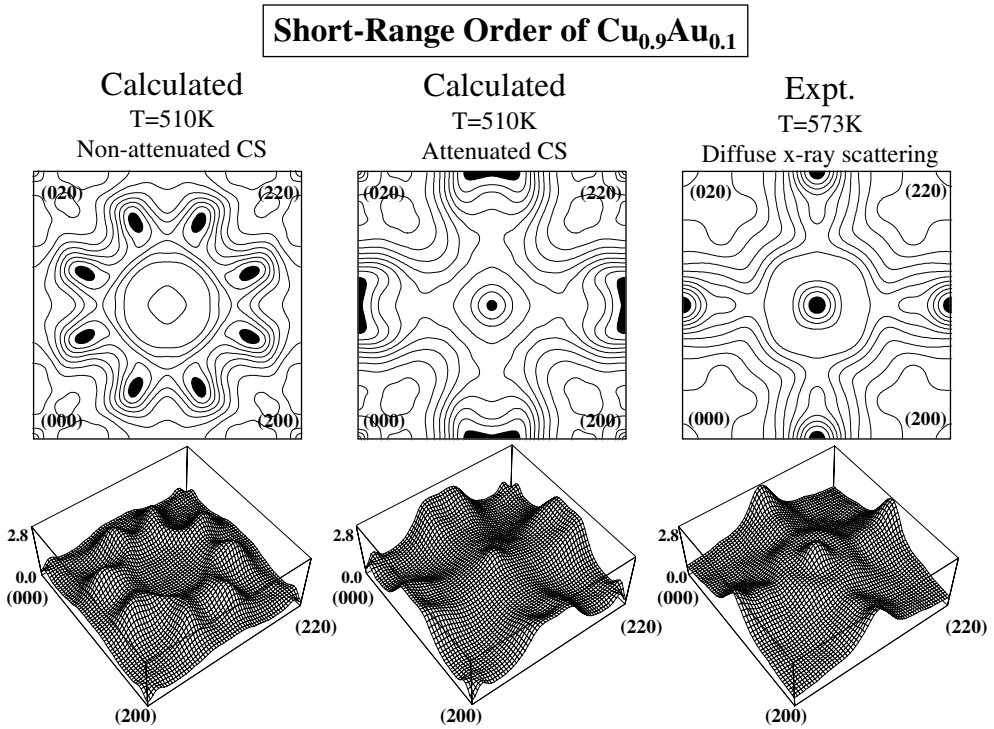

Figure 3. The calculated and measured [27] SRO patterns $\alpha(\boldsymbol{k})$ in $Cu_{0.90}Au_{0.10}$. Shown are the calculated results for both (a) non-attenuated coherency strain and (b) attenuated coherency strain and (c) the experimentally measured pattern extracted from diffuse x-ray scattering. SRO is shown in the $(hk0)$ plane, and peak contours are shaded black.

4.1. Type I alloy, Cu–Au: $\delta E_{ord} < 0 < \delta E_{CPS}$

Cu–Au is the prototypical ordering alloy system. Its compounds exhibit negative formation and mixing enthalpies, $\Delta H_{\mathrm{O}} < 0$, $\Delta H_{\mathrm{R}} < 0$ (see reference [18] for a recent compilation of the mixing and formation enthalpies in this system). The ordering energies are negative, $\delta E_{\mathrm{ord}} < 0$, as is the coherent phase-separation energy $\delta E_{\mathrm{CPS}} < 0$, placing this alloy into 'type I' of figure 1†. Figure 3 shows the calculated SRO $\alpha(\boldsymbol{k})$ for $Cu_{0.9}Au_{0.1}$. The SRO of this system has recently been measured [27] by means of diffuse x-ray scattering, and the measured results are also shown in figure 3 for comparison. As expected for a 'type I' alloy, the SRO shows ordering-type fluctuations (peaks in the SRO off the Γ point) consistent with the R $\rightarrow$ O arrow schematically illustrated in figure 1. The calculated SRO pattern with attenuated SRO is in quantitative agreement with the measured result [27], which also shows (100)-type SRO.

4.2. Type II alloy, Al–Mg: $\delta E_{ord} < 0 \sim \delta E_{CPS}$

The Al–Mg phase diagram shows a series of complex ordered compounds. Calculations for ordered Al–Mg compounds show [28, 29] that the low-energy fcc-based compounds have a negative formation enthalpy, $\Delta H_{\mathrm{O}} < 0$, whereas the mixing enthalpy of the solid-solution

† We have classified Cu–Au as 'type I' according to figure 1. However, it should be noted that the mixing energy of the completely random alloy in Cu–Au is nearly zero; only when the energetic effect of SRO is included does the mixing energy of the disordered solid solution become negative (see reference [18]).

phase is positive, $\Delta H_R > 0$, both from experiment [30] and theory [29]. First-principles calculations of the heat of solution of Mg impurities in Al also show a positive formation enthalpy [31]. Thus, the ordering energy is negative, and because the coherency strain energy is comparable to the mixing energy $\delta E_{CPS} \sim 0$; thus Al–Mg is a type II alloy. The calculated SRO of an $Al_{0.85}Mg_{0.15}$ solid solution is shown in figure 4. Table 1 shows that the cell-external relaxation energy of ordered Al–Mg compounds is nearly zero and that the relaxation is almost completely due to cell-internal relaxations. But, for structures with wavevectors near the Brillouin zone boundary such as an Al_1Mg_1 (001) superlattice, there are no cell-internal degrees of freedom, and thus the total relaxation energy is nearly zero (despite the fact that this cell is tetragonal). Hence, the relaxation tendencies in this system follow the attenuated form of equation (20), and thus we have performed the calculations for this system using the attenuated CS. The calculated SRO shows a clear ordering tendency with peaks at $\langle 100 \rangle$, despite the fact that $\Delta H_R > 0$. These (100) fluctuations in the solid solution are interesting since aged Al–Mg alloys show the existence of an ordered Al_3Mg ($L1_2$) phase in

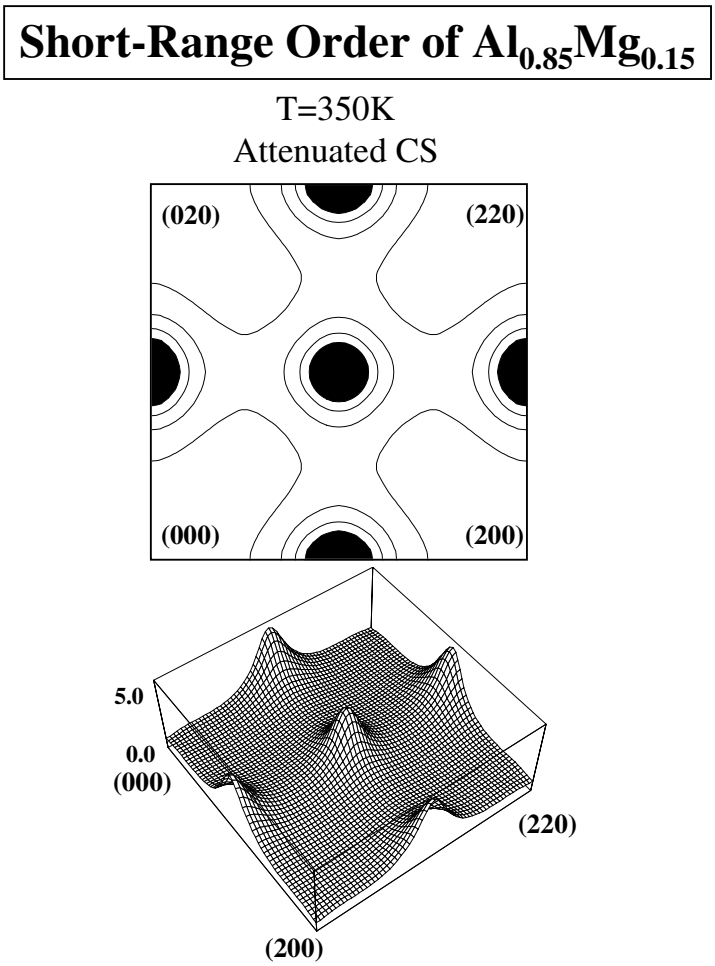

Figure 4. The calculated SRO patterns $\alpha(\boldsymbol{k})$ in $Al_{0.85}Mg_{0.15}$. SRO is shown in the $(hk0)$ plane, and peak contours are shaded black.

the precipitation sequence [29, 32], with this structure being composed of (100) composition waves. The metastable $L1_2$ phase does not appear in the Al–Mg phase diagram because the equilibrium phases are incoherent with the fcc Al matrix; however, in view of the existence of the $L1_2$ phase in coherent precipitation experiments, one might expect the metastable coherent phase diagram to contain this phase. Thus, the (100)-type fluctuations in the SRO are a reflection of the underlying coherent phase stability of the (100)-type Al_3Mg phase. Note that the calculated SRO fluctuations follow the R $\rightarrow$ O schematic diagram of figure 1. To our knowledge, there have been no measurements (diffuse scattering or otherwise) of the SRO in Al–Mg solid solutions.

4.3. Type III alloy, GaP–InP: $\delta E_{ord} < \delta E_{CPS} < 0$

The GaP–InP alloy system possesses positive formation enthalpies for all bulk structures, $\Delta H_{\mathrm{O}} > 0$, $\Delta H_{\mathrm{R}} > 0$, but a negative ordering energy, $\delta E_{\mathrm{ord}} < 0$ [8, 16, 21]. In other words, the formation enthalpy of low-energy ordered compounds is below that of the random alloy ($\delta E_{\mathrm{ord}} < 0$) as is the coherency strain energy ($\delta E_{\mathrm{CPS}} < 0$). (Surface ordering [22,33] is another effect whereby $\Delta H_{\mathrm{O}}^{\mathrm{bulk}} > 0$ in bulk but the constraint of coherent epitaxy (epi) changes the sign of $\Delta H_{\mathrm{O}}^{\mathrm{epi}} < 0$ near the surface.) Further, Lu *et al* [16] have shown that the SRO in this system is ordering, thus making it a type III alloy. Another previous study [34] suggests that Ti–V might be a type III alloy. Figure 5 shows the SRO calculated for $Ga_{0.5}In_{0.5}P$ using the cluster expansion of reference [21]. The calculations of figure 5 were obtained from a cluster expansion constructed from a 'ternary' valence-force-field model which was carefully fitted to a large database of LAPW formation enthalpies [21]. In contrast, the cluster expansion of reference [16] was directly fitted to LAPW energetics, with no force field as an intermediate step. Other than the GaP–InP cluster expansion used in figure 5, all other cluster expansions in this paper were constructed directly from first-principles total energies. The SRO of $Ga_{0.5}In_{0.5}P$ clearly shows an ordering tendency, with peaks at the $(1\frac{1}{2}0)$ positions, as found by Lu *et al* [16] The lowest-energy coherent ordered structures in the GaP–InP system correspond to (210)-type short-period superlattices, as these structures possess the optimal geometry for relaxation of tetrahedrally coordinated systems. The calculated SRO is a manifestation of these low-energy (210) structures, and corresponds to the R $\rightarrow$ O fluctuations, schematically illustrated in figure 1 for 'type III' alloys.

4.4. Type IV alloy, Ni–Au: $\delta E_{ord} \sim \delta E_{CPS} < 0$

Ni–Au alloys show positive formation enthalpies $\Delta H_{\mathrm{O}} > 0$, positive mixing enthalpies $\Delta H_{\mathrm{R}} > 0$, a miscibility gap in the phase diagram, and yet both measurements [4] and calculations [8, 15, 35] of the SRO of $Ni_{0.4}Au_{0.6}$ show peaks off the Γ point, just like for GaP–InP. However, in contrast with the case for GaP–InP, the CS energy in Ni–Au is slightly lower than that of the lowest-energy ordered phase. Thus, as illustrated in figure 1, there will be energetically favourable fluctuations in the random alloy towards both ordering (R $\rightarrow$ O) and coherent phase separation (R $\rightarrow$ CS). The competition between these two types of fluctuation distinguishes 'type IV' Ni–Au from 'type III' GaP–InP. In GaP–InP, only R $\rightarrow$ O fluctuations are energetically favourable, as the CS energy is much higher than that of the lowest-energy ordered phase.

Using an unattenuated form for the CS, we previously [15] calculated the SRO of Ni–Au alloys for the $Ni_{0.4}Au_{0.6}$ composition (where we could compare with experiment) as well as for other compositions where there are currently no measurements. Like that of the Cu–Au system, the CS energy of Ni–Au shows strong anharmonic effects, and the soft elastic direction

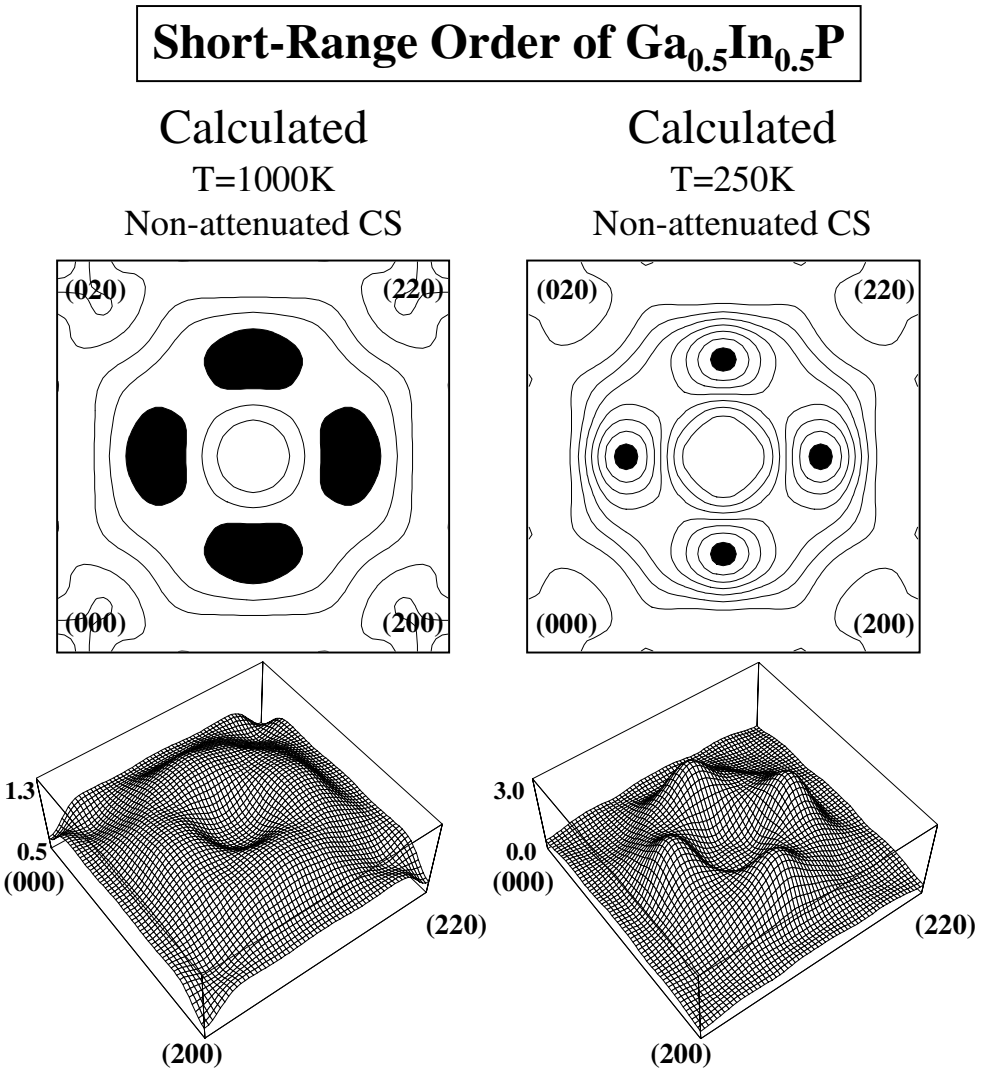

Figure 5. The calculated SRO patterns $\alpha(\boldsymbol{k})$ in $Ga_{0.50}In_{0.50}P$. SRO is shown in the $(hk0)$ plane, and peak contours are shaded black.

for Ni-rich alloys is (210) due to the elastic response of Au under compression. Thus, just like in figure 3 for Cu–Au, we found the unattenuated SRO calculation for Ni-rich Ni–Au alloys produced SRO peaks along the $\langle \xi \frac{\xi}{2} 0 \rangle$ direction. Because we have found this SRO to be incorrect for the Cu–Au alloys, we also want to re-examine the SRO for Ni-rich (and Au-rich) alloys and evaluate the effects of attenuating the CS for these alloys. Figure 6 shows the calculated SRO for $Ni_{0.75}Au_{0.25}$ both for unattenuated and attenuated CS. The SRO peaks change position when the more correct, attenuated form of the CS is used. The SRO shows peaks along the $(\xi 00)$ line, in accordance with the measured (and calculated) SRO peaks for $Ni_{0.40}Au_{0.60}$. Thus, the SRO in figure 6 with attenuated CS is a more accurate prediction of the SRO for *Ni-rich* Ni–Au alloys than our previous calculations [15]. However, the previous calculations of the SRO in *Au-rich* $Ni_{0.40}Au_{0.60}$ were in qualitative agreement with experiment.

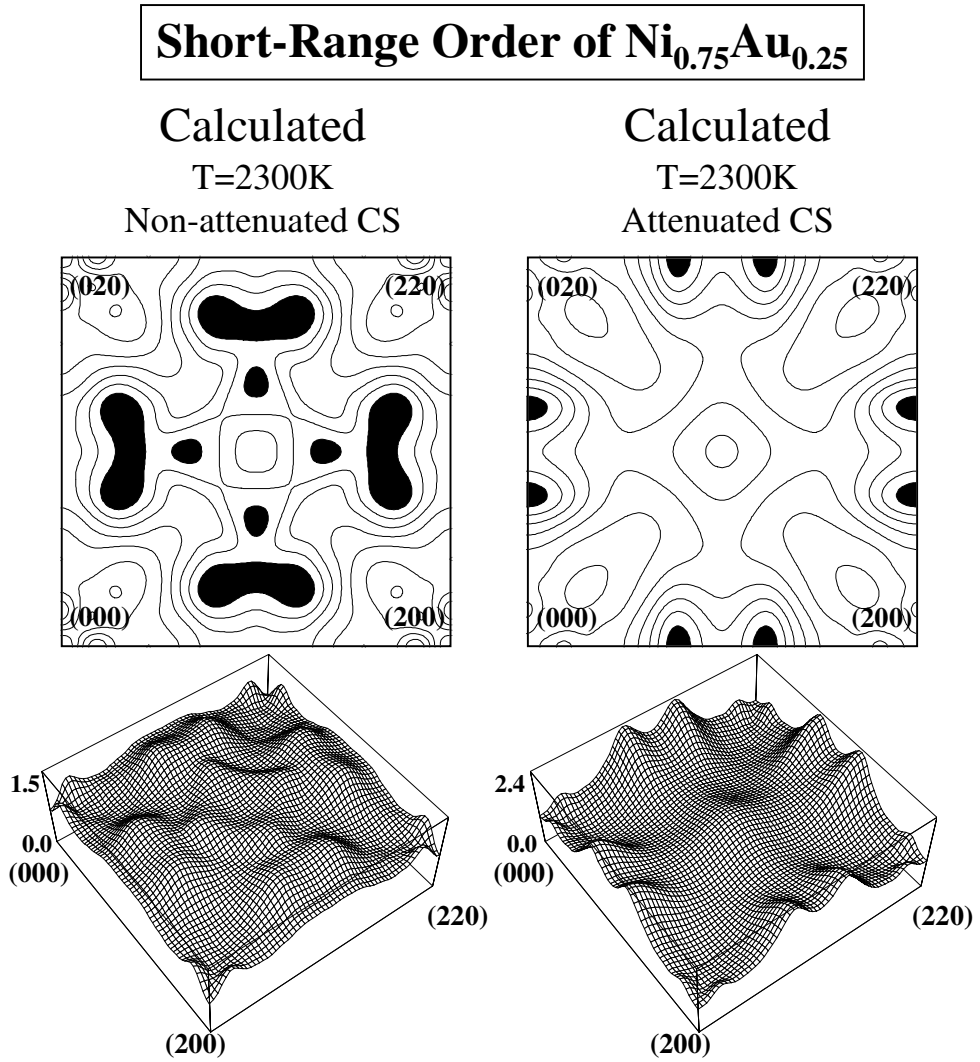

Figure 6. The calculated SRO patterns $\alpha(\boldsymbol{k})$ in $Ni_{0.75}Au_{0.25}$. Shown are the calculated results for both (a) non-attenuated coherency strain and (b) attenuated coherency strain. SRO is shown in the $(hk0)$ plane, and peak contours are shaded black.

Thus, it is important to see that attenuating the CS does not change the SRO peak position for Au-rich alloys. Figure 7 shows the calculated SRO for $Ni_{0.40}Au_{0.60}$. Clearly, for Au-rich alloys, the attenuation of the CS does not affect the SRO in a qualitative way, and leaves the calculated SRO in agreement with diffuse scattering measurements [4].

4.5. Type V alloy, Cu–Ag: $\delta E_{CPS} < \delta E_{ord} < 0$

Cu–Ag is a prototypical 'phase-separating' alloy, which exhibits positive formation enthalpies $\Delta H_{\mathrm{O}} > 0$, positive mixing enthalpies $\Delta H_{\mathrm{R}} > 0$, a miscibility gap, and a coherent phase-separated state that is *lower* in energy than both that of the random alloy and those of ordered

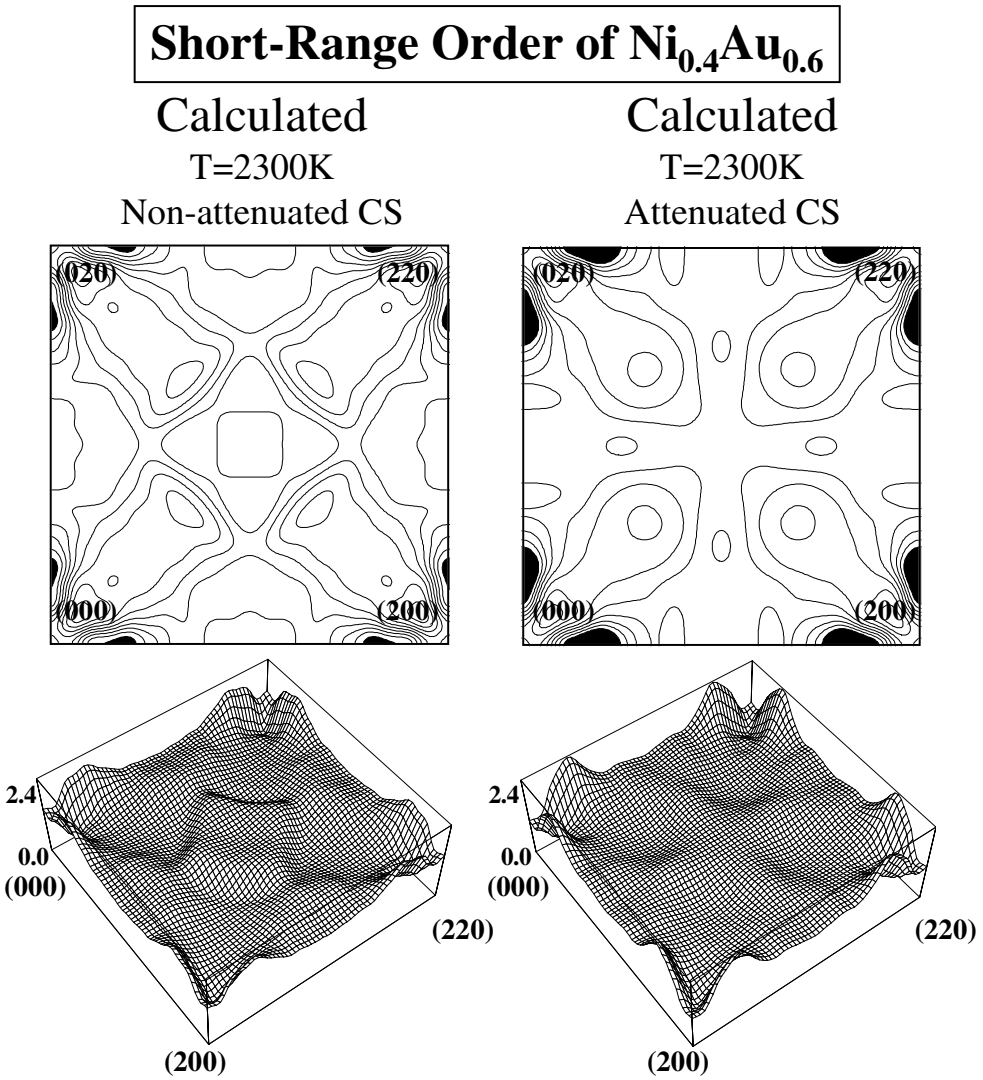

Figure 7. The calculated SRO patterns $\alpha(\boldsymbol{k})$ in $Ni_{0.40}Au_{0.60}$. Shown are the calculated results for both (a) non-attenuated coherency strain and (b) attenuated coherency strain. SRO is shown in the ($hk0$) plane, and peak contours are shaded black.

compounds. This latter fact distinguishes Cu–Ag from GaP–InP and Ni–Au. In GaP–InP, the CS energy is above that of ordered compounds, and in Ni–Au the CS energy is slightly below, but very close in energy to that of ordered compounds. The calculations of SRO in Cu–Ag have been discussed previously and the SRO was shown to be clustering (with peaks at Γ) [15]. In figure 8 we show the SRO for a $Cu_{0.95}Ag_{0.05}$ alloy at $T = 480$ K. Although this is a different composition and temperature than the calculations of reference [15], the SRO still shows clustering-type peaks at (000). The effect of attenuating the CS is not likely to have a significant effect since the attenuation does not affect the energetics near the Γ point, where the SRO shows peaks. Thus, for clustering alloys, the attenuated CS is likely to be unimportant.

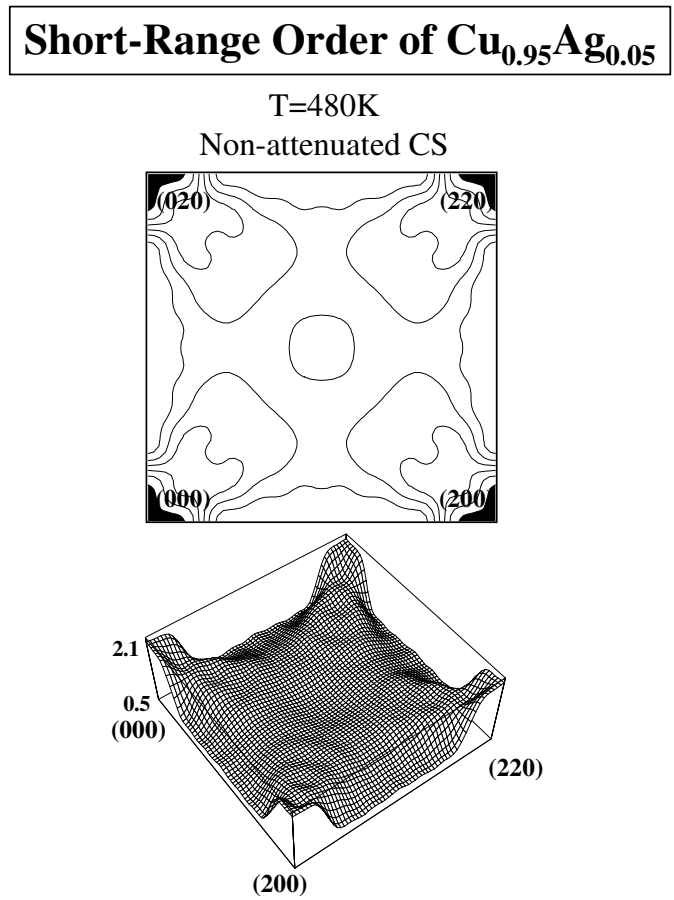

Figure 8. The calculated SRO pattern $\alpha(\boldsymbol{k})$ in $Cu_{0.95}Ag_{0.05}$. SRO is shown in the $(hk0)$ plane, and peak contours are shaded black.

5. Summary

Short-range order reflects an energetic competition between perfectly random and imperfectly random alloys *at the same composition*. In contrast, long-range order reflects not only this iso-compositional competition, but also an energetic competition between a compound at composition x, and its constituents at compositions $x = 0$ and $x = 1$ (and, more generally, between two-phase mixtures of compounds at any compositions). This simple picture enables us to divide SRO versus LRO behaviour of alloys into five generic groups:

(i) *Type I (most compound-forming systems, e.g., Cu–Au)*, where $\Delta H_O < 0$ (i.e., ordering-type LRO) and where $\Delta H_O < \Delta H_R$, so the random alloy can lower its energy by developing ordering-type SRO (figure 3). Thus, the dominant wavevectors $\boldsymbol{k}_{LRO}$ and $\boldsymbol{k}_{SRO}$ are both ordering type ($\boldsymbol{k} \neq 0$).

(ii) *Type II (e.g., Al–Mg)*, where $\Delta H_O < 0$ (i.e., ordering-type LRO) but $\Delta H_R > 0$ (unstable random alloy). Here too, the random alloy can lower its energy by developing ordering-type SRO patterns, even though $\Delta H_R > 0$ (figure 4). Again, both $\boldsymbol{k}_{LRO}$ and $\boldsymbol{k}_{SRO}$ are of ordering type.

(iii) *Type III (e.g., most semiconductor alloys and perhaps Ti–V)*, where $\Delta H_O > 0$ (i.e., phase-separating LRO) and $\Delta H_R > 0$ (unstable random alloy), but $\Delta H_O < \Delta H_R$. Here, the random alloy can lower its energy by adopting ordering-type SRO ($\boldsymbol{k}_{SRO} \neq 0$) even though the LRO is phase separating ($\boldsymbol{k}_{LRO} = 0$). Thus, $\boldsymbol{k}_{LRO} \neq \boldsymbol{k}_{SRO}$.

(iv) *Type IV (e.g., Ni–Au)*, where $\Delta H_O > 0$ (i.e., phase-separating LRO) and $\Delta H_R > 0$ (i.e., unstable random alloy), but $\Delta H_O < \Delta H_R$ (as in type III) *and* $\Delta E_{CS} < \Delta H_R$. Here, the random alloy can lower its energy in *two* channels: by developing fluctuations akin to those of the ordered phase ($\boldsymbol{k}_{SRO} \neq 0$) or fluctuations corresponding to phase separation ($\boldsymbol{k}_{SRO} = 0$).

(v) *Type V (most phase-separating materials, e.g., Cu–Ag)*, where $\Delta H_O > 0$ (i.e., phase-separating LRO), $\Delta H_R > 0$ (unstable random alloy) *and* $\Delta E_{CS} \ll \Delta H_O$. Here, the random alloy can lower its energy only by developing phase-separating fluctuations, so both $\boldsymbol{k}_{LRO}$ and $\boldsymbol{k}_{SRO}$ are of clustering type.

This classification scheme (figure 1) enables one to guess the qualitative SRO behaviour of an alloy given the measured or calculated enthalpies of ordered and random systems. It introduces three unusual cases (types II, III, and IV), in addition to the usual ordering (type I) and phase-separating (type V) cases. By noting that SRO reflects a constant-composition energy balance between two phases, one recognizes the possibilities of having ordering SRO coexisting with phase-separating LRO (type III).

To accurately calculate the short-range-order profile we utilize the first-principles mixed-bases cluster expansion (equation (10)), where the coherency strain energy is first separated out from the total energy, and the remainder ('chemical energy') which reflects the constant-composition term is expanded in (a momentum-space series of) pair interactions and in (a real-space series of) many-body interactions. We found here that in those alloy systems where the long-period structures (corresponding to $\boldsymbol{k} \to 0$) have relaxation energies for some ordering directions very different to those of the short-period structures (corresponding to $\boldsymbol{k} \to \pi/n$), a wavevector-dependent term $F(|\boldsymbol{k}|)$ must be introduced into the coherency strain to produce a balanced description. Examples include structures with very large size mismatch such as Cu–Au and Ni–Au, where anharmonic effects lead to large relaxation energies for a particular ordering direction in long-period structures, while short-period structures do not have such a large relaxation. $F(|\boldsymbol{k}|)$ then attenuates the $\boldsymbol{k} \to \pi/n$ relaxation energy with respect to that of $\boldsymbol{k} \to 0$. For phase-separating systems, where the SRO occurs near $\boldsymbol{k} = 0$, the function $F(|\boldsymbol{k}|)$ makes no change. Similarly, at the compositions where anharmonic effects are weak (Au-rich Ni–Au or Cu–Au), the $F(|\boldsymbol{k}|)$ function makes no changes even for size-mismatched alloys. We find that this new, attenuated form of the coherency strain, when combined with our first-principles cluster expansion, produces SRO patterns in excellent agreement with those from diffuse scattering experiments.

Acknowledgments

VO gratefully acknowledges support from the Office of Energy Research (OER) (Division of Materials Science of the Office of Basic Energy Sciences (BES)), US Department of Energy, under contract No DE-AC04-94-AL85000. Work performed at the National Renewable Energy Laboratory was supported by the Office of Energy Research (OER) (Division of Materials Science of the Office of Basic Energy Sciences (BES)), US Department of Energy, under contract No DE-AC36-98-GO10337.

References

[1] Schwartz L H and Cohen J B 1977 *Diffraction from Materials* (New York: Academic)
[2] Moss S C 1966 *Local Atomic Arrangements Studied by X-ray Diffraction* ed J B Cohen and J E Hilliard (New York: Gordon and Breach) pp 95–122
[3] Solal F, Caudron R, Ducastelle F, Finel A and Loiseau A 1987 *Phys. Rev. Lett.* **58** 2245
[4] Wu T B and Cohen J B 1983 *Acta Metall.* **31** 1929
[5] Reinhard L, Schönfeld B, Kostorz G and Bührer W 1990 *Phys. Rev.* B **44** 1727
[6] Reinhard L, Robertson J L, Moss S C, Ice G E, Zschack P and Sparks C J 1992 *Phys. Rev.* B **45** 2662
[7] Epperson J E, Anderson J P and Chen H 1994 *Metall. Mater. Trans.* A **25** 17
[8] Lu Z W and Zunger A 1994 *Phys. Rev.* B **50** 6626
[9] Wolverton C and Zunger A 1995 *Phys. Rev.* B **52** 8813
[10] de Fontaine D 1979 *Solid State Physics* vol 34 (New York: Academic) p 73
[11] Khachaturyan A G 1983 *Theory of Structural Transformations in Solids* (New York: Wiley)
[12] Müller S, Wolverton C, Wang L-W and Zunger A 1999 *Phys. Rev.* B **60** 16 448
[13] Laks D B, Ferreira L G, Froyen S and Zunger A 1992 *Phys. Rev.* B **46** 12 587
[14] Zunger A 1994 *NATO ASI on Statics and Dynamics of Alloy Phase Transformations* (New York: Plenum) p 361
[15] Wolverton C, Ozoliņš V and Zunger A 1998 *Phys. Rev.* B **57** 4332
[16] Lu Z-W, Laks D B, Wei S-H and Zunger A 1994 *Phys. Rev.* B **50** 6642
[17] Wolverton C and Zunger A 1995 *Phys. Rev. Lett.* **75** 3162
[18] Ozoliņš V, Wolverton C and Zunger A 1998 *Phys. Rev.* B **57** 6427
[19] Wolverton C 1999 *Phil. Mag. Lett.* **79** 683
[20] Wei S-H and Krakauer H 1985 *Phys. Rev. Lett.* **55** 1200
Singh D J 1994 *Planewaves, Pseudopotentials, and the LAPW Method* (Boston, MA: Kluwer)
[21] Wolverton C and Zunger A 1995 *Phys. Rev. Lett.* **75** 3162
[22] Ozoliņš V, Wolverton C and Zunger A 1998 *Phys. Rev.* B **57** 4816
[23] Peressi M and Baroni S 1994 *Phys. Rev.* B **49** 7490
[24] Debernardi A and Baroni S 1994 *Solid State Commun.* **91** 813
Debernardi A, Baroni S and Molinari E 1995 *Phys. Rev. Lett.* **75** 1819
[25] Leung K and Stechel E, unpublished
[26] Ferreira L G, Ozoliņš V and Zunger A 1999 *Phys. Rev.* B **60** 1687
[27] Schoenfeld B, Portmann M J, Yu S Y and Kostorz G 1999 *Acta Mater.* **47** 1413
[28] Narasimhan S and Davenport J W 1995 *Phys. Rev.* B **51** 659
[29] Wolverton C 2000 *Modell. Simul. Mater. Sci.* at press
[30] Brown J A and Pratt J N 1970 *Metall. Trans.* **1** 2743
Zuo Y and Chang Y A 1993 *CALPHAD* **17** 161
Ludecke D and Hack K 1986 *Z. Metallk.* **77** 145
[31] Chetty N, Weinert M, Rahman T S and Davenport J W 1995 *Phys. Rev.* B **52** 6313
[32] Sato T, Kojima Y and Takahashi T 1982 *Metall. Trans.* A **13** 1373
Osamura K and Ogura T 1984 *Metall. Trans.* A **15** 835
[33] Zunger A and Mahajan S 1988 *Handbook of Semiconductors* 2nd edn, ed S Mahajan (Amsterdam: Elsevier) p 133
[34] Reinhard L and Turchi P E A 1994 *Phys. Rev. Lett.* **72** 120
[35] Asta M and Foiles S M 1996 *Phys. Rev.* B **53** 2389